
Spatio-temporal evolution of fault networks : implications for deep radioactive waste disposal sites

K. Hardacre, O. Scotti

Institut de protection et sûreté nucléaire - Fontenay-aux-Roses - France

Abstract: The objective of this work is to provide estimates of both vertical and lateral propagation rates, on time scales of 100 000 years, for the faults systems known to be present today in the region of Bure, the site of an underground rock laboratory. The project is divided into three parts: 1) literature review (fault growth processes and data), 2) benchmarking against data a numerical code that allows for spontaneous development and growth of faults and 3) application to the Bure site. A brief overview of fault growth processes and observed fault propagation rates shows that non-negligible values (20-50 mm/yrs or roughly 5 km in 100 000 years) can be reached. Preliminary results obtained from two numerical simulations 1) fault growth of a pre-existing weaknesses and 2) fault growth of a spontaneously generated fault system, provide encouraging results with values that are comparable with those observed in nature for the growth of normal fault systems. The application to strike-slip system tha characterizes the Bure site is still underway.

1. INTRODUCTION

One of the key factors determining the choice of a site for underground radioactive waste storage facilities is the spatial organization of the fracture system and its potential evolution throughout the lifetime of the disposal site. This project will investigate the likelihood of fault activity (which could lead to seismic events) and fault growth (which could create connected fluid pathways) over time periods on the order of thousands of years. The literature on fault propagation is exclusively concerned with the growth of normal faults. The fracture network system of the Bure site is predominantly strike-slip in nature. A numerical model (BEW3D) based on a simple concept of stress transfer between faults allows to assess propagation rates in any kind of environment. After a brief description of the Bure site and a literature review of proposed growth processes and observed field data, preliminary results are presented concerning the benchmarking of this numerical model against field data.

2. THE BURE SITE

2.1. Data Sources

BRGM and several oil companies conducted geological studies of the Bure area before choosing it as the site for an underground rock laboratory. In addition to surface outcrops, 1300km of seismic data and 68 well logs were acquired. ANDRA has drilled 7 boreholes and conducted reconnaissance mapping of outcrops. IPSN has conducted several field studies and has produced a structural map for the region.

Existing Fractures

Outcrops reveal that major faults in the region are steeply dipping and that striations on fault planes observed in the field are consistent with a strike-slip sense of displacement (Cushing et al., 2001). As bedding is locally close to horizontal, it is difficult to obtain displacement estimates for even the largest structures. Thus displacement and distance to the nearest tip cannot be used to estimate a minimum fault size. Different interpretations of the fracture network are available for this site. The age of the faults is not known precisely and their potential activity in the future can only be speculated upon. Nevertheless, reasonable scenarios can be envisaged and will be tested in this project.

2.2. Stress and Strain Rate Environment

Strain rates in northeast France are no bigger than $2 \times 10^{-9} \text{ yr}^{-1}$ or more likely of the order $5 \times 10^{-17} \text{ s}^{-1}$ (Ward, 1998). No geodetic measurements north of the Alps have so far registered relative motions greater than the measurement uncertainties (Ward, 1998). Nevertheless, Nocquet et al. (20001) have shown that NW Europe is not a rigid block

2.3. Fault Propagation at Bure

The prime objective of this study is to estimate both vertical and lateral propagation rates for strike slip faults in interlayered limestones and marls at depths less than 1 km, over timescales of 100 000 years. Over such long time scales, the magnitude and direction of stresses and strains can change. Therefore, it will also be desirable to study the response of the existing faults to a stress field different to that which exists at the present day.

2. FAULT GROWTH PROCESSES

2.1. Defining fault growth

Faults are roughly planar features across which rocks are displaced. For a fault growing in isolation, the displacement is greatest at the centre and diminishes away from this point. A point at which the displacement is zero is called a tip. In this study, we consider fault growth to be the increase in fault surface area resulting from propagation of the tip line. Where a fault intersects and displaces the earth's surface, a fault scarp forms (Fig. 1). What is generally measured in the field is the rate at which the tip of the fault scarp propagates horizontally.

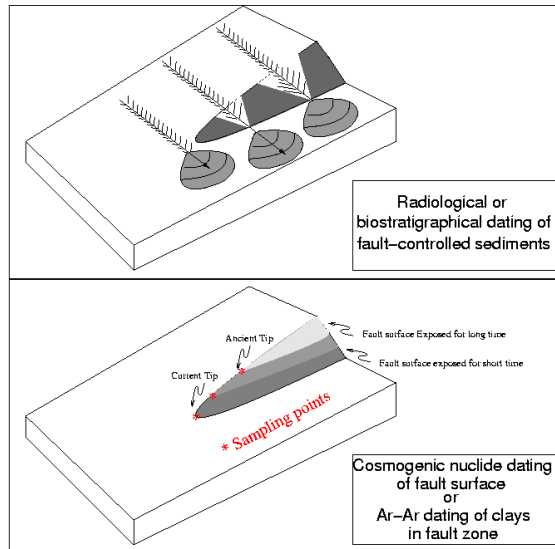


Figure 1 Cartoons illustrating idealized fault growth processes and geological means for observing it in the field.

2.2. Historical background

Faults were first described a few centuries ago (Davies 1879). How they came into being, how much displacement they accumulate and what determines their length are still open questions today. Over the past 20 years, the need to better understand the fracture system that control fluid flow in oil fields, has encouraged interest in fault growth processes (Cowie and Scholz, 1992; Walsh and Watterson, 1988). Since 1990 there has been a gradual yet fundamental shift in ideas about the growth and evolution of faults. Previously, growth models primarily focused on the propagation of a single isolated fault and the influence of rock properties on controlling displacement-length ratios for individual faults. The shift in perspective has been to consider instead the evolution of a population of faults forming during a particular tectonic episode (Davy et al., 1990; Sornette et al., 1990; Cowie et al., 1995). It is clear from field observations and analogue modelling that crustal deformation is accommodated by large numbers of faults rather than a single structure. Moreover deformation occurs at all scales from micro cracks to major faults that may penetrate the entire crust. It is now widely recognised that faults interact at both short-range and at long-range. These interactions are thought to play a key role determining the spatial organization of the deformation, i.e. the concentration of strain along fault zones with large displacements separated by regions that are less deformed (Sornette et al., 1990; Cowie et al., 1993, 1995).

2.3. Fault Growth in Isolation

A great deal of work has been done to understand the mechanics of faulting. The main problem for describing strain accumulation in the crust is the accumulation of permanent strain: at a gross scale the deformation may be successfully described by continuum models which assume, for example, a viscous or visco-elastic rheology for the lithosphere (England, 1983). However as faults are displacement discontinuities, their role as a deformation mechanism cannot be explicitly included in these continuum models. A second problem arises in trying to understand the generation and growth of a fault surface. The formation and growth process cannot be fully described using traditional fracture mechanics models because it involves distributed inelastic deformation, in particular fracturing, of the surrounding rock (Cox and Scholz, 1988). In spite of the inherent complexities of faulting, it is observed that larger (longer) faults have more displacement on them than smaller (shorter) faults. This is consistent with faults growing, i.e. the length of a fault increasing as displacement accumulates on the fault.

In the approach taken by Cowie and Scholz (1992) a fault accumulates displacement through repeated earthquakes. During a single earthquake, the maximum slip is only a few metres, and yet there are faults that have several hundred metres of displacement, and so faults must accumulate displacement and grow over many earthquake cycles. They asked the question "For a certain increase in the amount of displacement, by how much would the fault grow? Through a series of empirical relations, they show that, for a constant moment release rate \dot{M}_0 , time t , elastic shear modulus μ and the ratio of maximum displacement to length γ , fault length L can be estimated roughly by

$$L = \sqrt[3]{\frac{3\dot{M}_0 t}{\mu\gamma}} \quad \text{Eq. 1}$$

2.3.1. Results for Bure

According to this very simple approach which assumes that all the deformation takes place along a single fault, it is possible to estimate a worst case scenario: standard values for the

material parameters ($\mu=3 \times 10^{10} \text{ Nm}^{-2}$, $\gamma=6 \times 10^{-2}$) and for an appropriate moment release rate for northeast France ($M_0=5 \times 10^{14} \text{ Nmyr}^{-1}$, extrapolated from figure 3 of Ward (1998)), Eq. 1 suggests that a faults on the order of 5 km long could be generated in 100 000 years.

3. FIELD OBSERVATIONS

3.1. From individual faults

Observations of fault growth are rare; because faults generally grow during earthquakes and, with repeat times of large earthquakes measured in 100s or 1000s of years, demonstrating incremental fault growth over a few earthquake cycles is difficult. Nevertheless different approaches have been developed using: 1) Displacement of dated markers; 2) Extent of fault-controlled sedimentary depocentres; 3) Length of time for which different parts of a fault scarp have been exposed to the atmosphere (cosmogenic dating); 4) Dating oldest and youngest minerals that developed during fault growth (radiometric dating). Figure 1 illustrates two of these methods.

Method 1 has only been used to measure lateral propagation rates of normal faults. Methods 2 and 3 require the existence of a fault scarp at the Earth's surface, so they are difficult to apply to strike-slip faults. Ar-Ar is the most appropriate radioactive dating scheme for minerals normally developing during faulting (micas at depth or clay minerals in the near surface environment). As the errors associated with this technique are large (of the order of 1Ma) Method 4 can only be used for exceedingly long-lived faults. Published data on growth rates for natural faults are exclusively for large, dip-slip faults in tectonically very active regions. For each published study, fault propagation rates and regional strain rates are summarized in Table 1.

Moorewood and Roberts (1999) measured the lateral propagation rate of the South Alkynodies Fault in the Gulf of Corinth using Method 1. They estimated the lateral propagation rate of a large normal fault at the earth's surface by looking at dated, displaced paleo-shorelines. Manighetti et al. (2001) also used the offset of contemporaneous sediments and volcanic rocks to date the lateral propagation of large normal faults in the Afar region of East Africa.

By using Method 2, Jackson and Leeder (1994) estimated the lateral propagation rate of the Pierce Fault in the Basin and Range Province, USA. They inferred the position of the fault tip in the past by examining the dated alluvial fan sediments left by channels cutting through the fault scarp. Jackson et al. (1996) also used the fact that fault scarps affect drainage and deposition systems (Method 2) to estimate the propagation rate of active faults in Otago, New Zealand. They observed features such as wind gaps and gorges that had been uplifted by a height H while the fault propagated a distance L . They then estimated how many earthquakes would be required to cause an uplift H , assuming each earthquake ruptured the entire fault surface. Thus, they obtained propagation rates in terms of "metres per event". One would need additional data in the form of earthquake recurrence intervals to express these propagation rates in terms of "metres per year". Method 2 was also used by Contreras et al. (2000) who, by examining fault-scarp controlled depocentres in Lake Malawi, identified the position of the lateral tip of a large normal fault at several points in the past.

Zreda & Noller (1998) used Method 3 to investigate prehistoric earthquakes on the Hebgen Lake Fault (Montana, USA). The concentrations of cosmogenic ^{36}Cl were used to date how long different parts of the fault scarp had been exposed to the atmosphere. On fault scarps the ^{36}Cl exposure age is the time since the scarp face was suddenly exposed during a large earthquake. From their figures 1 and 3, one can calculate that the southerly tip of the Hebgen Lake Fault propagated by approximately 5km in 37Kyr.

Method 4 was used by Foster & Gray (1999) to investigate the propagation rates of a thrust fault in the Lachlan Orogen, Eastern Australia. The fault was large (dip-slip displacements

on the order of 1000km) and long lived (60My) and so fault growth rates could be obtained by radiometrically dating micas that crystallised in the fault zone as it developed.

Authors	Present Day Fault Length (km)	Fault Propagation Rate (mm/yr)	Regional Strain Rate (yr^{-1})
Moorewood & Roberts (1999)	15	12.1 - 16.7	1×10^{-6}
Manighetti et al. (2001)	0.006 - 1.3	2 - 20	$3 - 9 \times 10^{-6}$
Jackson & Leeder (1994)	20	10	3×10^{-8} ♥
Jackson, Norris & Youngson (1996)	30	15-45m per M6 event	
Contreras, Anders & Scholz (2000)	100	13	$1 \times 10^{-16} - 1 \times 10^{-15}$ ♦
Zreda & Noller (1998)	34	135*	1×10^{-8} ♣
Foster & Gray (1999)	1000+	8	1×10^{-15}

Table 1. Fault propagation rates in the published literature. Note that the data are exclusively for large, dip-slip faults in high strain areas. * Erosion of the upper part of the fault scarp can lead to over estimates. Rates from ♥Thatcher et al. (1999), ♦Morley (1994) ♣Rate from Wernicke et al. (2000)

3.1.1. Results for Bure

The lateral propagation rates of large, dip-slip faults measured at the earth's surface in high strain rate areas (Table 1) provide upper bounds to the lateral and vertical propagation rates that may be expected for small strike-slip faults in the sub-surface in the low-strain rate region of Bure.

3.2. From a population of faults

Field observations and analogue modelling have shown that deformation is accommodated by a large number of faults with a range of sizes. In isolation, fault growth rate is controlled by the mechanical properties of the host material and the remote loading rate. However, where faults are not isolated, the growth on one fault may be affected by the presence of another fault nearby or elsewhere in the deforming region (see Willemse et al. 1996 for a good review of dip slip faults, Aydin and Schultz (1990) for examples of interactions between strike-slip faults). For example, McLeod et al. (2000) and Walsh et al. (2001) both studied syn-tectonic faults in the North Sea basin. They observed that, at the start of deformation, there were many small faults all of which were growing, but after several millions of years, many of the faults had become inactive while a few others were still growing.

Data shows that faults are born, grow, interact and link up. The question now is: "What scenarios can be expected for the strike-slip system of Bure?" . Some insight into this question may be gained through the use of simple numerical models.

4. NUMERICAL MODELLING OF A POPULATION OF FAULTS

The following paragraph is just an illustration of the modelling approaches that exist in the literature, far from being a comprehensive review.

4.1. Plastic yielding criterion

Hardacre (2000), using a 2D finite element code, simulated normal faulting in a heterogeneous, plastic medium in cross section over 100 000 years. She observed that four factors controlled fault population evolution in her models:

- the distribution of yield strengths

- the initial stress field
- the stress drop associated with failure
- the shape and size of stress perturbations after failure

4.1.1. Results

Upward propagation rates for major faults in these models were of the order of 0.07 mm/yr for regional extensional strain rates of $3 \times 10^{-7} \text{yr}^{-1}$.

4.2. Mohr-Coulomb criterion

Cowie (1998) suggested a reason why the growth of one fault is affected by the presence of other faults nearby: stress feedback. King et al. (1994) demonstrated that slip on a fault perturbs the surrounding stress field, bringing some areas closer to failure and taking other areas further from failure. The pattern of stress enhancement zones and stress shadow zones around a strike slip fault is shown in Figure 2. Stress feedback increases the frequency of failure of favourably aligned faults, and so stimulates the growth of such faults and causes strain localisation.

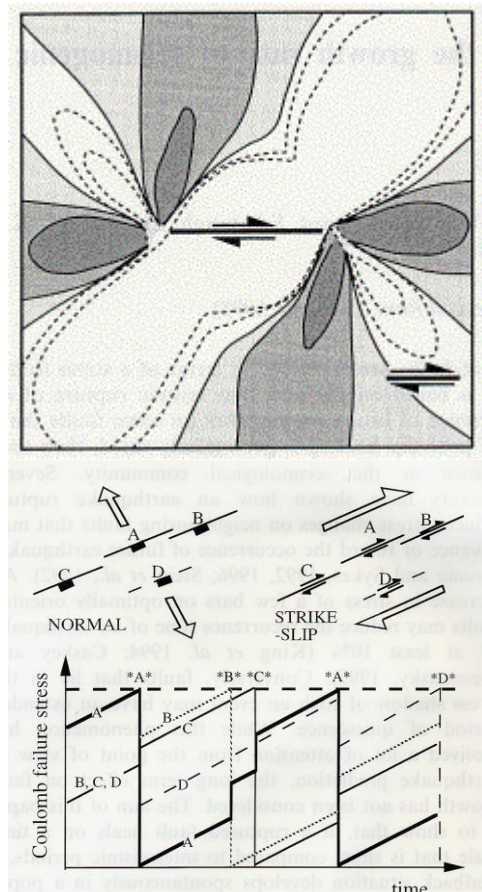


Figure 2. The change in coulomb failure stress (a measure of how far from failure is a particular location) resulting from a strike slip event: Clearly, areas along strike are brought closer to failure (loaded=black); elements in other locations are taken further from failure (unloaded=white). The right figure shows the load on four faults A,B, C

and D through time. Whilst the failure of A loads B and C, it unloads D. When B fails, then re-loads A and D. Consequently, the faults A, B and C fail more frequently than D, and so they grow more quickly (from Cowie 1998).

For stress feedback to work faults must recover their pre-slip strength (they must heal) quickly and stress perturbations must persist over timescales comparable with the recurrence time. Laboratory studies (Olsen et al., 1998) suggest that faults heal over very short timescales.

5. BENCHMARKING OF MODELS AGAINST DATA

5.1. Objectives

The literature is dominated by data on lateral propagation of normal faults over timescales of millions of years. The model used in this study is capable of simulating any type of faulting in three dimensions. Benchmarking of this model against real data is necessary before using it to simulate faulting at Bure.

5.2. The Numerical Model

We use the BEWE3D (Maillot et al. 1998) in which fractures appear and develop spontaneously in a 3D, heterogeneous, brittle, linear-elastic media. Failure is determined by the Mohr-Coulomb criteria, cohesion is the only parameter that varies in space. Failure is modelled as an absolute drop in shear stress. Fluids, non-elastic rheologies, thermal effects and rupture dynamics are not considered.

Boundary conditions in BEWE3D are periodic in all three dimensions. This means that gravitational effects (lithostatic pressure gradients) and free-surface effects cannot be incorporated in to this model. The static stress field following a failure event is calculated by using the finite difference method to integrate with respect to time the equations of motion. The theoretical basis of this model is discussed in detail in Maillot et al., 1998 and summarized in the appendix.

5.3. Numerical Implementation

The deformation of the material proceeds in two nested cycles: i) the loading cycle and ii) the rupture cycle. In the loading cycle, the uniform strain rates are applied until a single node reaches failure, as determined by the Mohr-Coulomb criterion. The model then enters the rupture cycle: deviatoric stress drops in the breaking node and the stress tensors in the surrounding nodes augment. The static stress state resulting from a single node failure is calculated before testing for rupture elsewhere in the mesh. When no further ruptures occur, the rupture cycle ends and the loading cycle resumes to trigger the next failure.

6. BENCHMARKING RESULTS

6.1. Growth of a pre-existing Weakness

In this simulation, we aim to examine the lateral propagation rate of a pre-existing weak zone, growing in antiplane shear (normal faulting). The elastic parameters were selected to mimic limestone; a stress drop of 4MPa was imposed and a strain rate of 10^{-15} s^{-1} was used (similar to the exemple of Contreras et al., 2000). Each rupture event corresponded to an

earthquake of magnitude -4.7 ($M_0 = \mu * A * \Delta u$, $\mu = 3 \times 10^{10}$, $A = 5 \times 5 \text{m}$, $\Delta u = 4 \times 10^{-5}$; $M_s = \log(M_0) - 12.23$ – Ward(1998)). To generate a cohesion map, values were selected randomly from a uniform frequency distribution between 5 and 15MPa. Then, in a zone 3 nodes wide and 61 nodes long at the centre of the mesh, the cohesions were reduced to 30% of this randomly assigned value (Fig. 3). The initial length of the weak zone or “fault” was 305m and, after $225 \times 10^9 \text{s}$ (7130 years), the left tip had propagated by 155m and the right tip by 115m. This yields a propagation rate of roughly 20mm/yr and 15mm/yr respectively. Note how the deformation is concentrated around the tips of the weakened zone.

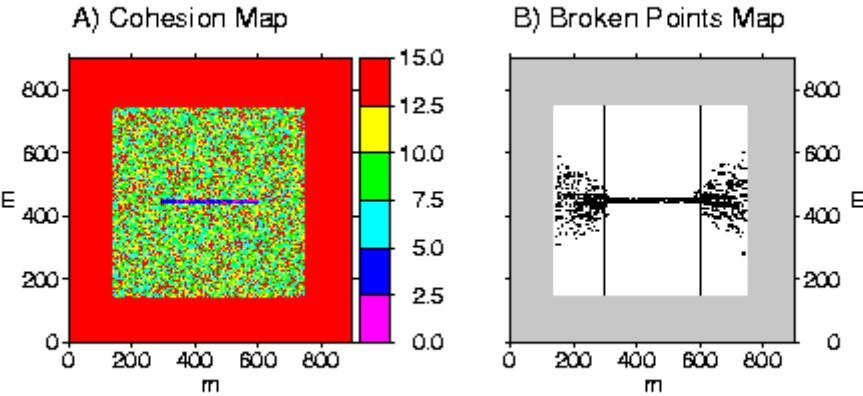


Figure 3. a) Cohesion map showing the pre-existing weakness at the centre of the model, b) Broken points after 350 ruptures (229×10^9 seconds). The weakened zone and interpreted fault tips are highlighted.

6.2. Spontaneous Fault Growth

This simulation is the same as that predicted above, except that the cohesion map did not have a pre-existing weak zone. After $238 \times 10^9 \text{s}$ (200 ruptures) the largest structure that developed is 50m long (Fig. 4). This is equivalent to a tip-propagation rate of roughly 3 mm/yr.

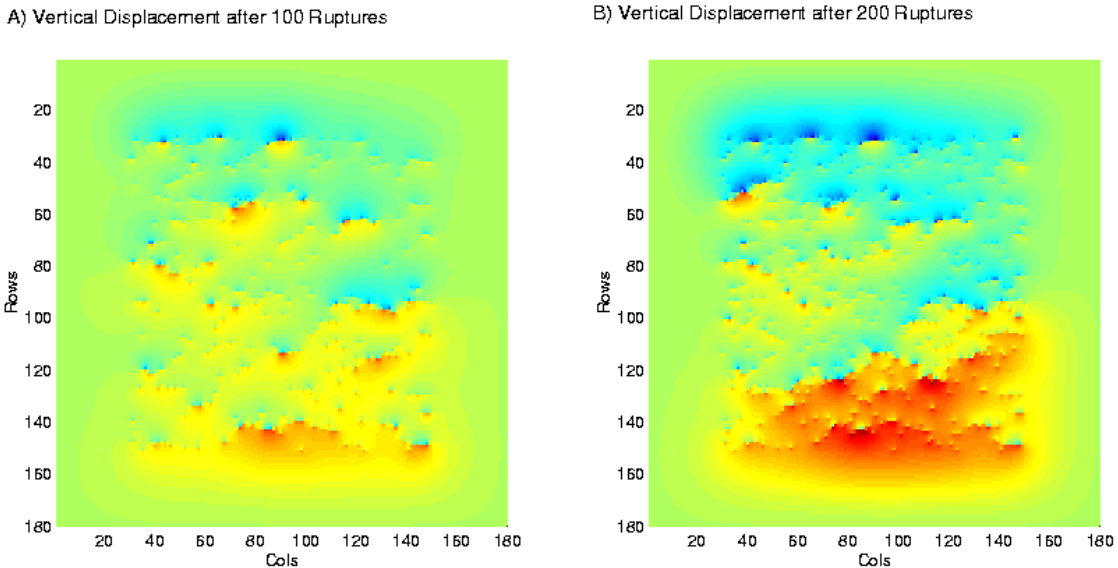


Figure 4 Spontaneous normal fault generations in a heterogeneous medium.

6.3. Comparing Simulations with Theory and Measurements for Lateral Propagation Rates of Normal Fault

The simulations results for East Africa show propagation rates that vary between 3 to 20mm/yr, comparable to the 13 mm/yr observed by Contreras et al. (2000). If we apply the Cowie and Scholz (1992) approach, where a single spontaneously-generated fault is assumed to release all the seismic moment (Eq. 1), the predicted propagation rate for East Africa is of ~60 mm/yr, clearly an upper limit.

7. CONCLUSIONS

Literature on fault growth rates is dominated by data for large, long-lived normal faults and so, to test the validity of the BEWE3D model, we decided to simulate the growth of normal faults, before simulating the strike-slip faults in the Bure region. Preliminary simulations with both pre-existing weaknesses and with spontaneously generated faults suggest that fault propagation rates in the model are comparable with values observed in nature. Therefore, the lateral propagation rates of large, dip-slip faults measured at the earth's surface in high strain rate areas (Table 1) provide upper bounds to the lateral and vertical propagation rates that may be expected for small strike-slip faults in the sub-surface in the low-strain rate region of Bure. However, the effect of model parameters such as stress drop, cohesion distribution, grid spacing and buffer region needs to be fully investigated before going further with predictive modelling at Bure.

APPENDIX

1. Constitutive laws

At all times at any point in the medium not undergoing failure, stresses and strains are linearly related by Hooke's Law

$$\sigma_{ij}(x, t) = c_{ijkl}(x)\epsilon_{kl}(x, t). \text{Eq 2}$$

The media is homogeneous and isotropic media, (c_{ijkl} does not depend on position x)

$$c_{ijkl} = \lambda\delta_{ij}\delta_{kl} + \mu(\delta_{ik}\delta_{jl} + \delta_{il}\delta_{jk}). \text{Eq 3}$$

where δ_{ij} is the Kroenecker delta and λ and μ are the Lamé parameters, which are specified via the P-wave and the S-wave velocities of the medium

$$V_p = \sqrt{\frac{\lambda + 2\mu}{\rho}},$$

$$V_s = \sqrt{\frac{\mu}{\rho}}. \quad \text{Eq 4}$$

2. Loading

The total stress in a deforming material consists of two parts: i) a homogeneous part that contains a pre-stress component (e.g. lithostatic stress and other stresses present at the start of the experiment) plus a loading component, and ii) an inhomogenous part that embodies the perturbing effects of the faults in the medium. The total stress has the form

$$\sigma_{ij}^H(x, t) = \sigma_{ij}^H(t) + \sigma_{ij}^F(x, t) \quad \text{Eq 5}$$

and the homogeneous part of the stress field can be expressed as

$$\sigma_{ij}^H(x,t) = \sigma_{ij}^H(0) + t * f(i,j) * c_{ijkl} * \dot{\epsilon}_{kl} \quad \text{Eq 6}$$

where t is time since the start of the experiment, and f(i,j) is a function with values 1 or 0 depending on whether the i,j component of the loading stress is applied or not.

3. Failure Criteria

The Mohr-Coulomb criterion is used to determine when and where shear fracture will occur in the material (note, failure in tension is not considered):

$$\tau = C + \nu\sigma_n \quad \text{Eq 7}$$

$$|\tau| = C + \nu\sigma_n,$$

where τ is the absolute value of the shear stress on the plane, C is cohesion, ν is the coefficient of internal friction and σ_n is the normal stress on the fault plane. Using Mohr's circles for representing stress, failure can be understood as the moment at which the largest circle intersects the failure line, which is defined by the cohesion and the angle of internal friction. A node fails when the distance to rupture function, d_{rupt} , in that node is zero.

$$d_{rupt} = C \cos \varphi + \sigma_n \sin \varphi - \tau \quad \text{Eq 8}$$

where φ is the angle of internal friction. The Mohr-Coulomb criteria also gives the orientation of the failure plane relative to the orientation of the principal stresses. All medium properties are constant in space and time, except cohesion, which varies in space. It is hence the only heterogeneity of the medium. The default spatial distribution is a uniform frequency distribution arranged in a random, uncorrelated pattern in space.

4. Stress Drop

Maximum stress drop is a constant. However, when rupture starts, the stress drop is not instantaneous but makes a smooth transition from zero to its maximum value over a time t_r . The evolution of shear stress on the fracture plane can then be written as

$$\sigma_{ij}(x^b, t > t_0) = g(t)\sigma_{ij}(x^b, t_0) \quad \text{Eq 9}$$

where x^b is a location, t_0 is the time of failure and σ_{ij} is the deviatoric stress, defined as

$$\sigma_{ij} = \sigma_{ij} - \frac{1}{3}\delta_{ij}\sigma_{kk}, \quad \text{Eq 10}$$

and $g(t)$ is a sine-shaped function.

5. Stresses, strains and displacements resulting from slip

The deviatoric stress on the fracture plane falls according to the equation above, but the other parts of the stress tensor evolve freely according to the equations of motion and the constitutive relation (Hooke's Law). Cauchy's equation of motion

$$\rho \frac{\partial^2 u_i}{\partial t^2} = \nabla_j \sigma_{ij} \quad \text{Eq 11}$$

relates the stresses in the medium σ_{ij} to the displacement field u and the rock density ρ . This equation is solved using the method of finite differences, to find the static state i.e.

$$\nabla_j \sigma_{ij} = 0 \quad \text{Eq 12}$$

REFERENCES

1. Ackermann, R., Withjack, M. & Schlische, R. (2001) The geometric and statistical evolution of normal fault systems: an experimental study of the effects of mechanical layer thickness on scaling laws. *Journal of Structural Geology* (in press)
2. Aydin, A. & Schultz, R.A. 1990 Effect of mechanical interactions on the development of strike-slip faults with echelon patterns. *Journal of Structural Geology* 12 123-129;
3. Cushing E. M., Lemeille F., Lozac'h et K. Hardacre Examen microstructural préliminaire de l'environnement régional du laboratoire souterrain de Bure, Rapport IPSN/DPRE/SERGD 01-18, 20001.
4. D'Agostino, N. Guiliani, R. Mattone, M. & Bonci, L. 2001 Active crustal extension in the central Apennines (Italy) inferred from GPS measurements in the interval 1994-1999. *Geophysical Research Letters* V28, N10, 2125-2128.
5. Davies, A. T., The phenomena of heaves of faults in the mineral veins of St. Agnes, Cornwall, Appendix, Ann. Rep., 47, R. Cornwall Polytech. Soc., 1879.
6. Borgos, H., Cowie, P. & Dawers, N. (2001) Practicalities of extrapolating 1D fault and fracture size-frequency distributions to higher dimensional samples. *Journal of Geophysical Research*, 105, B12, 28,377-28,392.
7. Casarotti, E., Piersanti, A., Lucente, P. & Boschi, E. 2001 Global postseismic stress diffusion and fault interaction at long distances. Abstracts with Program, European Geophysical Society Annual Meeting, 2001.
8. Chinnery, M.A., 1969 Theoretical fault models. *Publications of the Dominion Observatory*, 17, 211-223
9. Contreras, J., Anders, M. & Scholz, C. 2000 Growth of a normal fault system: observations from the Lake Malawi basin of the East African Rift. *Journal of Structural Geology*, 22 (1), 159-168
10. Cowie, P.A. & Scholz, C.H. 1992 Fault growth by the accumulation of seismic slip. *Journal of Geophysical Research*, 97, B7, 11085-11095.
11. Cowie, P.A. 1998 A healing-reloading feedback control on the growth rate of seismogenic faults. *Journal of Structural Geology* 20, 1075-1087.
12. Davy, P., Hansen, A., Bonnet E. and S-Z Zhang, Localisation and fault growth in layered brittle-ductile systems: implications for deformation of the continental lithosphere. *Journal of Geophysical Research* 100, 6281-6289, 1995.
13. Foster, D.A. and Gray, D.R. 1999 Deformation rates and timing of deformation in the western Lachlan Orogen, eastern Australia. *Geological Society of America, 1999 Annual Meeting Abstracts with Programs - Geological Society of America* 31 (7) 301.
14. Hardacre, K. M. 2000 Controls on fault network evolution and population statistics- insights from field studies and numerical modelling. Unpubl. PhD thesis, University of Edinburgh, U.K.
15. Hazzard, J.F. 1999 Numerical modelling of acoustic emissions and dynamic rock behaviour. Unpubl. PhD thesis, Keele University, UK
16. Jackson, J. & Leeder, M. 1994 Drainage systems and the development of normal faults: an example from Pleasant Valley, Nevada. *Journal of Structural Geology* 16, 1041-1059.
17. Jackson, J. Norris, R. & Youngson, J. 1996 The structural evolution of active fault and fold systems in central Otago, New Zealand: evidence revealed by drainage patterns. *Journal of Structural Geology* 18 (2/3), 217-234.

18. Maillot, B., Cowie, P. & Lague, D. 1998 Simulating polyphase faulting with a tensorial 3D model of fault growth. In: G. Jones, Q.J. Fisher and R.J. Knipe (eds) *Faulting, Fault Sealing and Fluid Flow in Hydrocarbon Reservoirs*. Geological Society, London, Special Publications, 147, 209-216.
19. Manighetti, I., King, G.C.P., Gaudemer, Y., Scholz, C.H. and Doubre, C. 2001 Slip accumulation and lateral propagation of active normal faults in Afar. *Journal of Geophysical Research* 106, B7, 13,667-13,696.
20. McLeod, A.E., Dawers, N.H. and Underhill, J.R. 2000 The propagation and linkage of normal faults: insights from the Strathspey-Brent-Statfjord fault array, northern North Sea. *Basin Research*, 12, 263-284.
21. Moorewood, N. & Roberts, G. 1999 Lateral propagation of the surface trace of the South Alkyonides normal fault segment, central Greece: its impact on models of fault growth and displacement-length relationships. *Journal of Structural Geology* 21, 635-652.
22. Morley, C.R. 1994 Interaction of deep and shallow processes in the evolution of the Kenya Rift. *Tectonophysics* 236, 81-91.
23. Okada, Y. 1992 Internal deformation due to shear and tensile faults in a half-space. *Bulletin of the Seismological Society of America*, 82, 1018-1040.
24. Olsen, M.P., Scholz, C.H. and Léger, A. 1998 Healing and sealing of a simulated fault gouge under hydrothermal conditions: implications for fault healing. *Journal of Geophysical Research* 92, B1, 345-355.
25. Prenskey, S.E. 1999 Advances in borehole imaging technology and applications In: Lovell, M; Williamson, G; Harvey, P (eds) *Borehole imaging; applications and case histories*. Geological Society Special Publication 159: 1-43.
26. Sornette, D Davy, P and Sornette A., Structuration of the lithosphere as a self-organised critical phenomenon. *Journal of Geophysical Research* 95, 17353- 17361, 1990.
27. ten Veen and Klienspehn, 2000 Quantifying the timing and sense of fault dip slip: New application of biostratigraphy and geohistory analysis. *Geology*, 28,5, 471-474.
28. Thatcher, W., Foulger, G. R., Julian, B. R., Svarc, J., Quilty, E. & Bawden, G.W. 1999 Present day deformation across the Basin and Range Province, Western United States, *Science*, 282, pp. 1,714-1,718.
29. Walsh, J.J., Childs, C., Imber, J., Manzocchi, T., Watterson, J. & Nell, P.A.R., 2001. Strain localisation and population changes during fault system growth. Submitted to *Journal of Structural Geology*
30. Walsh, J.J. and J. Watterson, Analysis of the relationship between displacements and dimensions of faults, *Journal of Structural Geology*, 10, 238-247, 1988.
31. Ward, S.N. 1998 On the consistency of earthquake moment release and space geodetic strain rates: Europe. *Geophysics Journal International*, 135, 1011-1018.
32. Wells & Coppersmith, 1994 New empirical relationships among magnitude, rupture length, rupture width, rupture area, and surface displacement. *Bulletin of the Seismological Society of America* 84,4, 974-1002
33. Wernicke, B., Friedrich, A.M., Niemi, N.A., Bennett, R.A. & Davis, J.L. 2000 Dynamics of plate boundary fault systems from Basin and Range geodetic network (BARGEN) and geologic data *GSA Today*, v. 10, no. 11
34. Willemsse, E.J.M. Pollard, D.D. & Aydin, A. 1996 Three-dimensional analyses of slip distributions on normal fault arrays with consequences for fault scaling. *Journal of Structural Geology*, 18, 295-309.

35. Wright, T. Parsons, B. & Fielding, E. 2001 Measurement of interseismic strain accumulation across the North Anatolian Fault by satellite radar interferometry. *Geophysical Research Letters* V28, N10, 2117-2120.
36. Ziolkowski, A. 1999 Multiwell imaging of reservoir fluids *The Leading Edge*, December 1999, 1371-1376.